8-21-2017

Broadband near-field infrared spectroscopy with a high temperature plasma light source

D. J. Lahneman
College of William and Mary, djlahneman@email.wm.edu

T. J. Huffman
College of William and Mary

Peng Xu
College of William and Mary

S. L. Wang
College of William and Mary

T. Grogan
College of William and Mary

See next page for additional authors

Recommended Citation

Lahneman, D. J.; Huffman, T. J.; Xu, Peng; Wang, S. L.; Grogan, T.; and Qazilbash, M. M., Broadband near-field infrared spectroscopy with a high temperature plasma light source (2017). *OPTICS EXPRESS*, 25(17). 10.1364/OE.25.020421

Research Article | Vol. 25, No. 17 | 21 Aug 2017 | OPTICS EXPRESS 20421
Optics EXPRESS

Broadband near-field infrared spectroscopy with a high temperature plasma light source

D. J. LAHNEMAN,* T. J. HUFFMAN, PENG XU, S. L. WANG, T. GROGAN, AND M. M. QAZILBASH

Department of Physics, College of William and Mary, Williamsburg, VA 23187-8795, USA
**djlahneman@email.wm.edu*

Abstract: Scattering-type scanning near-field optical microscopy (S-SNOM) has enormous potential as a spectroscopy tool in the infrared spectral range where it can probe phonon resonances and carrier dynamics at the nanometer lengths scales. However, its applicability is limited by the lack of practical and affordable table-top light sources emitting intense broadband infrared radiation in the 100 cm^{-1} to 2,500 cm^{-1} spectral range. This paper introduces a high temperature plasma light source that is both ultra-broadband and has much more radiant power in the infrared spectral range than conventional, table-top thermal light sources such as the globar. We implement this plasma lamp in our near-field optical spectroscopy set up and demonstrate its capability as a broadband infrared nano-spectroscopy light source by obtaining near-field infrared amplitude and phase spectra of the phonon resonances of SiO_2 and $SrTiO_3$.

OCIS codes: (180.4243) Near-field microscopy; (120.0120) Instrumentation, measurement, and metrology; (300.6340) Spectroscopy, infrared; (240.0240) Optics at surfaces.

References and links

1. R. Hillenbrand, T. Taubner, and F. Keilmann, "Phonon-enhanced light matter interaction at the nanometre scale," Nature **418**(6894), 159–162 (2002).
2. H. A. Bechtel, E. A. Muller, R. L. Olmon, M. C. Martin, and M. B. Raschke, "Ultrabroadband infrared nanospectroscopic imaging," Proc. Natl. Acad. Sci. U.S.A. **111**(20), 7191–7196 (2014).
3. F. Keilmann and R. Hillenbrand, "Near-field microscopy by elastic light scattering from a tip," Philos Trans A Math Phys Eng Sci 362(1817), 787–805 (2004).
4. E. E. Bell, "Measurement of the far infrared optical properties of solids with a michelson interferometer used in the asymmetric mode: Part 1, mathematical formulation," Infrared Phys. **6**(2), 57–74 (1966).
5. R. Hillenbrand and F. Keilmann, "Complex optical constants on a subwavelength scale," Phys. Rev. Lett. **85**(14), 3029–3032 (2000).
6. M. Brehm, A. Schliesser, F. Cajko, I. Tsukerman, and F. Keilmann, "Antenna-mediated back-scattering efficiency in infrared near-field microscopy," Opt. Express **16**(15), 11203–11215 (2008).
7. L. M. Zhang, G. O. Andreev, Z. Fei, A. S. McLeod, G. Dominguez, M. Thiemens, A. H. Castro-Neto, D. N. Basov, and M. M. Fogler, "Near-field spectroscopy of silicon dioxide thin films," Phys. Rev. B **85**(7), 075419 (2012).
8. Z. Fei, G. O. Andreev, W. Bao, L. M. Zhang, A. S McLeod, C. Wang, M. K. Stewart, Z. Zhao, G. Dominguez, M. Thiemens, M. M. Fogler, M. J. Tauber, A. H. Castro-Neto, C. N. Lau, F. Keilmann, and D. N. Basov, "Infrared nanoscopy of dirac plasmons at the graphene-SiO_2 interface," Nano Lett. **11**(11), 4701–4705 (2011).
9. I. M. Craig, M. S. Taubman, A. S. Lea, M. C. Phillips, E. E. Josberger, and M. B. Raschke, "Infrared near-field spectroscopy of trace explosives using an external cavity quantum cascade laser," Opt. Express **21**(25), 30401–30414 (2013).
10. S. Amarie and F. Keilmann, "Broadband-infrared assessment of phonon resonance in scattering-type near-field microscopy," Phys. Rev. B **83**(4), 045404 (2011).
11. S. Bensmann, F. Gaußmann, M. Lewin, J. Wüppen, S. Nyga, C. Janzen, B. Jungbluth, and T. Taubner, "Near-field imaging and spectroscopy of locally strained GaN using an IR broadband laser," Opt. Express **22**(19), 22369–22381 (2014).
12. B. T. O'Callahan, W. E. Lewis, S. Möbius, J. C. Stanley, E. A. Muller, and M. B. Raschke, "Broadband infrared vibrational nano-spectroscopy using thermal blackbody radiation," Opt. Express **23**(25), 32063–32074 (2015).
13. F. Huth, M. Schnell, J. Wittborn, N. Ocelic, and R. Hillenbrand, "Infrared-spectroscopic nanoimaging with a thermal source," Nat. Mater. **10**(5), 352–356 (2011).
14. P. Hermann, A. Hoehl, P. Patoka, F. Huth, E. Rühl, and G. Ulm, "Near-field imaging and nano-Fourier-transform infrared spectroscopy using broadband synchrotron radiation," Opt. Express **21**(3), 2913–2919 (2013).
15. P. Hermann, A. Hoehl, G. Ulrich, C. Fleischmann, A. Hermelink, B. Kästner, P. Patoka, A. Hornemann, B.

#300834 https://doi.org/10.1364/OE.25.020421
Journal © 2017 Received 27 Jun 2017; revised 6 Aug 2017; accepted 8 Aug 2017; published 14 Aug 2017

Optics EXPRESS

Beckhoff, E. Rühl, and G. Ulm, "Characterization of semiconductor materials using synchrotron radiation-based near-field infrared microscopy and nano-FTIR spectroscopy," Opt. Express **22**(15), 17948–17958 (2014).
16. J. M. Bridges and A. L. Migdall, "Characterization of argon arc source in the infrared," Metrologia **32**(6), 625–628 (1995).
17. F. Huth, A. Chuvilin, M. Schnell, I. Amenabar, R. Krutokhvostov, S. Lopatin, and R. Hillenbrand, "Resonant antenna probes for tip-enhanced infrared near-field microscopy," Nano Lett. **13**(3), 1065–1072 (2013).
18. A. L. McIntosh, B. A. Wofford, R. R. Lucchese, and J. W. Bevan, "High resolution Fourier transform infrared spectroscopy using a high temperature argon arc source," Infrared Phys. Technol. **42**(6), 509–514 (2001).
19. M. Fäth, S. Freisem, A. A. Menovsky, Y. Tomioka, J. Aarts, and J. A. Mydosh, "Spatially inhomogeneous metal-insulator transition in doped manganites," Science **285**(5433), 1540–1542 (1999).
20. T. Becker, C. Streng, Y. Luo, V. Moshnyaga, B. Damaschke, N. Shannon, and K. Samwer, "Intrinsic inhomogeneities in manganite thin films investigated with scanning tunneling spectroscopy," Phys. Rev. Lett. **89**(23), 237203 (2002).
21. M. M. Qazilbash, M. Brehm, B.-G. Chae, P.-C. Ho, G. O. Andreev, B.-J. Kim, S. J. Yun, A. V. Balatsky, M. B. Maple, F. Keilmann, H.-T. Kim, and D. N. Basov, "Mott transition in VO_2 revealed by infrared spectroscopy and nano-imaging," Science **318**(5857), 1750–1753 (2007).
22. A. S. McLeod, E. van Heumen, J. G. Ramirez, S. Wang, T. Saerbeck, S. Guenon, M. Goldflam, L. Anderegg, P. Kelly, A. Mueller, M. K. Liu, I. K. Schuller, and D. N. Basov, "Nanotextured phase coexistence in the correlated insulator V_2O_3," Nat. Phys. **13**(1), 80–87 (2016).
23. Y. Abate, D. Seidlitz, A. Fali, S. Gamage, V. Babicheva, V. S. Yakovlev, M. I. Stockman, R. Collazo, D. Alden, and N. Dietz, "Nanoscopy of phase separation in $In_xGa_{1-x}N$ alloys," ACS Appl. Mater. Interfaces **8**(35), 23160–23166 (2016).
24. C. Westermeier, A. Cernescu, S. Amarie, C. Liewald, F. Keilmann, and B. Nickel, "Sub-micron phase coexistence in small-molecule organic thin films revealed by infrared nano-imaging," Nat. Commun. **5**, 4101 (2014).
25. J. Stiegler, Y. Abate, A. Cvitkovic, Y. Romanyuk, A. Huber, S. Leone, and R. Hillenbrand, "Nanoscale IR absorption spectroscopy of individual NPs enabled by scattering-type near-field microscopy," ACS Nano **5**, 6494–6499 (2011).
26. W. G. Spitzer, R. C. Miller, D. A. Kleinman, and L. E. Howarth, "Far infrared dielectric dispersion in $BaTiO_3$, $SrTiO_3$, and TiO_2," Phys. Rev. **126**(5), 1710–1721 (1962).
27. M. K. Gunde, ""Vibrational modes in amorphous silicon dioxide," Phys. B Condens," Matter **292**, 286–295 (2000).
28. A. Cvitkovic, N. Ocelic, and R. Hillenbrand, "Analytical model for quantitative prediction of material contrasts in scattering-type near-field optical microscopy," Opt. Express **15**(14), 8550–8565 (2007).
29. M. F. Kimmitt and G. B. F. Niblett, "Infra-red emission from the theta pinch," Proc. Phys. Soc. **82**(6), 938–946 (1963).
30. W. Elenbaas, *Light Sources (Philips Technical Library)*, 1st ed. (Crane, 1973).

1. Introduction

Circumventing the diffraction limit of light using scattering-type scanning near-field optical microscopy (S-SNOM) has proven to be a powerful technique for probing the local nanoscale optical properties of solids. Its recent applications as a nano-imaging tool have employed mid-infrared frequencies while circumventing the diffraction limit by nearly three orders of magnitude [1,2]. By using broadband illumination with asymmetric Fourier transform infrared (FTIR) spectroscopy, local near-field spectra with nanometer scale spatial resolution have been obtained [3–5]. S-SNOM is based on an atomic force microscope (AFM) operated in tapping mode in which light is focused on to the metallic AFM tip in close proximity to the sample. The tip- sample interaction is encoded in the scattered optical signal which is then measured in the far-field with a photodetector. The ratio of the backscattered power compared to the incident power at the tip is $\eta_B \approx 0.02$, and the useful near-field signal is an even smaller fraction f_N of η_B, estimated to be $f_N \approx 0.003$ for a standard tip over gold [6]. Since the ratio of the scattered near-field signal to incoming light at the tip is so small, it is necessary to use high intensity light sources.

Broadband nano-spectroscopy in the far- and mid-infrared spectral range is challenging because of the limitations of existing high intensity light sources. The use of tunable, monochromatic lasers allows for high signal but is limited by the available wavelengths and obtaining a high-resolution broadband spectrum requires significant time [7]. Quantum cascade lasers (QCLs) have been implemented with S-SNOM and have the ability to quickly scan through wavelengths but have a narrow spectral range [8,9]. Difference frequency

Optics EXPRESS

generation provides a stable high intensity beam in the mid-infrared but needs to be tuned to different wavelength ranges to get the full spectrum and currently has a low frequency cutoff of ~550 cm^{-1} (18 μm wavelength) [10,11]. Thermal blackbody light sources like the globar provide a large spectral bandwidth but low intensities. Hence, significant integration time is required to obtain data with a globar and there is no usable intensity below ~750 cm^{-1} for broadband S-SNOM [12,13]. Previously, a globar was implemented as a broadband infrared source in our own near-field experimental setup. We were able to resolve phonon resonances in SiO_2 and SiC in the mid-infrared but the signal-to-noise level was very low and integration times of a few hours were required. Synchrotron light sources provide spatially coherent intense broadband light that is currently the highest intensity and widest bandwidth infrared source for nano-spectroscopy [2,14,15]. However, experiments require beam time at the synchrotron that is highly competitive to obtain and is generally of limited duration. Moreover, travel and accommodation costs are generally borne by the users. These issues make it challenging to do in-depth, long-term studies on samples at synchrotron beamlines, and also make it difficult to implement modifications and improvements to equipment that are better suited for table top set-ups.

A wall stabilized plasma light source has shown potential as a high intensity broadband light source in both the far-field and the near-field. However, there is only one published work using this light source for near-field infrared spectroscopy. Moreover, the startup procedure for this light source requires a manual shorting of the arc, there are reports of "violent sputtering episodes" at the anode, and the required input power to sustain the arc is on the order of kilowatts [16–18]. The most common type of commercial plasma light sources are the xenon high pressure plasma lamps which are useful as a broadband source for the near-infrared, visible and ultraviolet i.e. frequencies higher than 2,500 cm^{-1}. However, these lamps do not provide intensity in the mid- and far-infrared due to the plasma being encased in a quartz bulb which is opaque to these wavelengths. There is a need for a practical and affordable table-top light source that is ultra-broadband and covers the spectral range of ~100 cm^{-1} – 2,500 cm^{-1} to allow the exploration of materials at the nanoscale by probing infrared-active phonon resonances and electronic properties.

Infrared spectroscopy has been commonly used to probe infrared-active phonons and charge dynamics in materials. However, many materials have been shown to exhibit phase coexistence at length scales much smaller than the diffraction limit of infrared light. Infrared nano-spectroscopy techniques are necessary to properly understand the charge and lattice dynamics of these nano-domains that exist in a number of materials, for example, the oxides of vanadium and manganese as well as in the ternary alloy $In_{1-x}Ga_xN$ [19–23]. Recently, an S-SNOM setup has demonstrated that there is nanoscale phase coexistence of two crystallographic phases known as the thin film phase and bulk phase of pentacene [24]. It is shown through nano-imaging and point spectroscopy in the mid-infrared that there is bulk phase nucleation of pentacene during the growth of the expected thin film phase as well as during sample storage. In the mid-infrared it has been shown that the local absorption spectrum of silicon nitride nanoislands can be observed using S-SNOM [25]. To have the ability to probe nanoscale domains with broadband infrared spectroscopy in the far-infrared and mid-infrared spectral range would allow these types of experiments to be performed on a number of materials to discover and explore nanoscale phenomena that may also have significant potential for applications. Researchers will be able to probe the crystallinity of thin films over a broad spectral range, allowing the testing of the effectiveness of different growth methods. Moreover, the technique can be employed for nanoscale identification of materials, and quality control and characterization of nano-devices.

In this work, we introduce a new table-top light source that has significant potential as a broadband high intensity source of mid-infrared and far-infrared frequencies for microscopy applications. Our electrode stabilized argon plasma light source (APLS) is described, and its emission spectrum is characterized using an FTIR spectrometer and compared to the well-

Optics EXPRESS

known globar source. Then we employ the APLS for broadband nano-spectroscopy in the mid-infrared spectral range by resolving the phonon-polariton resonance in SiO_2 using a calibration grating of 100 nm of SiO_2 on Si (μmasch TGXYZ02). Finally, we demonstrate this argon plasma lamp's potential as a far-infrared light source by resolving a phonon-polariton resonance in bulk, crystalline strontium titanate ($SrTiO_3$). The spectra measured at room temperature are compared to the point dipole model and the finite dipole model using known literature values for the dielectric functions of SiO_2 and $SrTiO_3$ [26–28].

2. Experiment

2.1 Argon plasma light source (APLS)

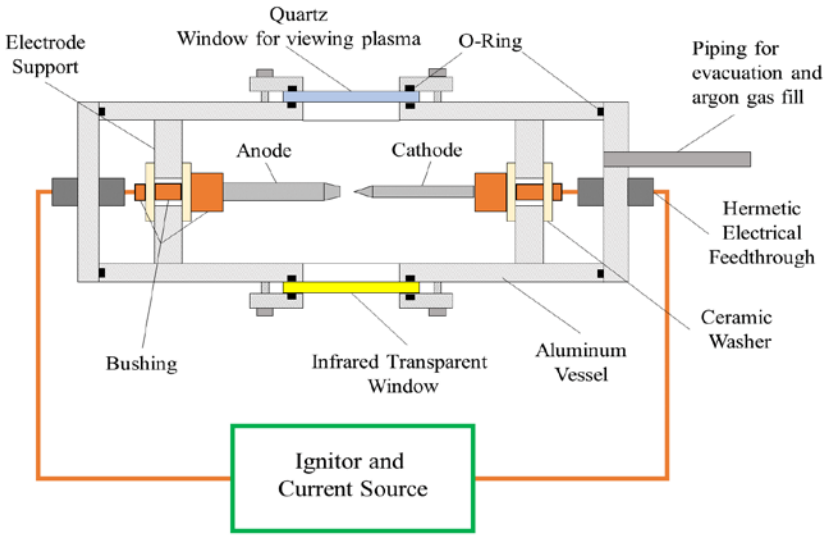

Fig. 1. A schematic representation of the APLS. A top view cross-section of the APLS is shown.

A noble gas plasma radiates bremsstrahlung (or free-free radiation) that is primarily from deceleration of free electrons due to interactions with ions, atoms and other electrons [29]. From the near-infrared to the ultra-violet, there is a continuum of bremsstrahlung radiation as well as intense, discrete atomic emission lines whose frequencies depend on the noble gas. In the far-infrared and much of the mid-infrared there is also significant continuum bremsstrahlung radiation but fewer atomic emission lines. Our home-built, electrode stabilized APLS has been constructed similar to a conventional short-arc lamp. One important difference from the conventional short-arc lamp is that the APLS is housed inside a sealed aluminum vessel with an infrared transparent window to allow access to the mid-infrared and far-infrared frequencies. A schematic representation of the APLS can be seen in Fig. 1. A high voltage pulse is applied to two tungsten electrodes 2 mm apart in high purity argon gas at a gauge pressure of one atmosphere. This causes an arc discharge to occur between the electrodes which is then sustained by a current of about 7 amperes. The input power to this lamp is about 90 W. The electrodes are in thermal contact with the water-cooled aluminum vessel but electrically isolated from it. A potassium bromide (KBr) or zinc selenide (ZnSe) window is clamped to the vessel to allow for infrared optical access to the plasma emission. Viton o-ring seals are used for isolating the high purity argon gas inside the vessel from atmospheric contamination. The light emission from the plasma is steered into a port of our Bruker Vertex 80v FTIR spectrometer using two off-axis parabolic mirrors. The first parabolic mirror collimates the beam which is then filtered through a germanium disk to eliminate the unwanted near-infrared and visible portion of the spectrum. The spectrum is

Optics EXPRESS

measured using a KBr beam splitter and a liquid nitrogen cooled Mercury-Cadmium-Telluride (MCT) photoconductor (Infrared Associates) with a KRS-5 window, and a 1 mm x 1 mm element.

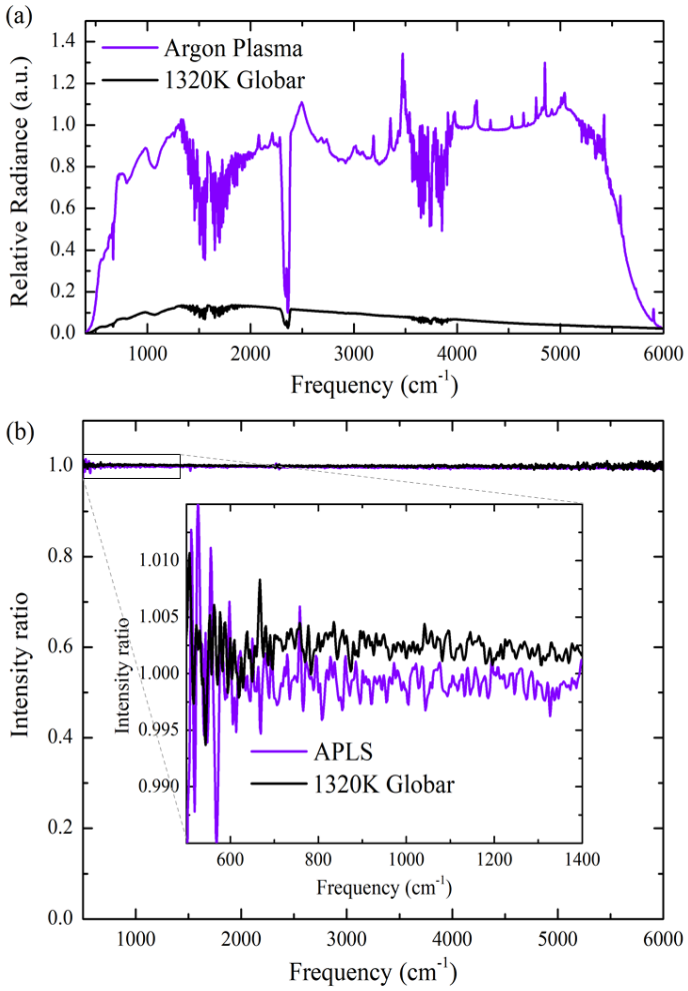

Fig. 2. (a) Relative radiance of the argon plasma (violet) compared to a 1320 K globar (black). The spectra were obtained with the Bruker Vertex 80v FTIR spectrometer in air. Sharp peaks in the APLS spectrum are mainly due to argon emission lines and the valleys are mainly due to atmospheric absorption. The atmospheric absorption features also appear in the globar spectrum. (b) Comparison of 100% lines taken with the Globar and APLS. (Inset) Zoomed in view of 100% lines demonstrating the relative noise levels of both sources in our spectral range of interest.

In Fig. 2(a), we plot the measured spectrum of the APLS. In the same figure, we also plot the spectrum of the globar source which radiates as a 1320 K blackbody. The globar spectrum was measured without the germanium filter. The absolute transmission of the germanium filter was also measured in the FTIR spectrometer. The lower cutoff of the APLS spectrum at ~500 cm^{-1} is due to the KBr beam splitter, the MCT detector, and ZnSe window of the APLS, and the upper cutoff at ~5,800 cm^{-1} is due to the germanium disk. The APLS spectrum displayed in Fig. 2(a) has been corrected for the reduced transmission through the ZnSe window and the germanium disk to demonstrate the radiance of the plasma relative to that of the globar. This was done so that the radiance of the plasma can be seen independent of the

Optics EXPRESS

choice of window and filter. The radiance of the APLS plasma in the region below 1000 cm^{-1} ranges from about 7 to 10 times that of the globar. Based on this relative radiance, we say that our effective plasma temperature is about 9000 K or higher. By taking the ratio of two successive measurements of the spectrum, 100% lines were obtained (Fig. 2(b)) to demonstrate the stability of the APLS compared to that of the globar. The APLS demonstrates highly stable intensity suitable for spectroscopy and microscopy rivaling the stability of the globar. The APLS is a highly stable light source because of the effective suppression of convection currents. The data from the APLS shown in Fig. 2 establishes this source's potential as an intense and stable mid-infrared and far-infrared light source. It is expected that there is significant intensity in the far-infrared below our lower measurement cutoff frequency [29]. Finally, due to the "short arc" electrode stabilized geometry of our lamp, the "hot spot" of the plasma, a volume that has the highest infrared emission, is estimated to be about 300 to 500 μm in diameter. This means that the APLS is closer to a point source than a globar making it more suitable for microscopy applications [30].

2.2 Broadband near-field infrared spectroscopy

The nano-spectroscopy setup primarily consists of a commercial S-SNOM from Neaspec GmbH and our APLS. Figure 3(a) shows a schematic representation of our beam path. The light from the hot spot of our argon plasma is collected and collimated with an off axis parabolic mirror with a 2 inch focal length. It is then incident on an indium tin oxide (ITO) coated glass planar mirror with a 45 degree angle of incidence. The ITO mirror significantly reduces the unwanted near-infrared and visible portion of the spectrum in the reflected light. Thereafter, the beam is focused through a 300 μm pinhole by a second 4 inch focal length off-axis parabolic mirror to improve the spatial coherence of our beam and to ensure we are aligned to the hot spot of the plasma. After the pinhole, the light beam is collimated using a one inch focal length off axis parabolic mirror, setting the beam diameter to ~10mm, and sent into our broadband S-SNOM system. The beam power after the pinhole is measured to be ~0.8 mW in the spectral range between 400 cm^{-1} and 5,800 cm^{-1}.

The S-SNOM set-up consists of an atomic force microscope employing a metallic coated AFM tip and an asymmetric FTIR interferometer. The incoming collimated infrared beam is incident on a ZnSe beam splitter sending part of the beam to the movable reference mirror and the other part of the beam to a parabolic mirror which is used to bring the beam to a focus on the tip and to collect and collimate the backscattered light. The backscattered and the reference beams are recombined at the beam splitter and brought to a focus on a liquid nitrogen cooled MCT detector. For the SiO_2 sample we use an AFM tip with a radius of about 15 nm (Arrow-NCPt) and a liquid nitrogen cooled photovoltaic MCT (Kolmar KLD-0.1-J1/208) with a ZnSe window and a spectral bandwidth of 750cm^{-1} – 3000 cm^{-1}. For the $SrTiO_3$ (STO) sample we use a liquid nitrogen cooled broadband photoconductive MCT (Infrared Associates FTIR-22-0.100) with a spectral bandwidth of 450 cm^{-1} – 5,000cm^{-1}. This is a similar detector to the one used with the Bruker in the far-field but has a 0.1 mm x 0.1 mm element size, a KBr window with moisture-resistant coating, and a preamp with 1 MHz bandwidth. Due to the lower detectivity of the broadband photoconductive MCT compared to the narrowband photovoltaic MCT, we used a larger 50 nm radius tip (PPP-NCSTAu) to enhance the near-field signal when measuring the STO sample.

Optics EXPRESS

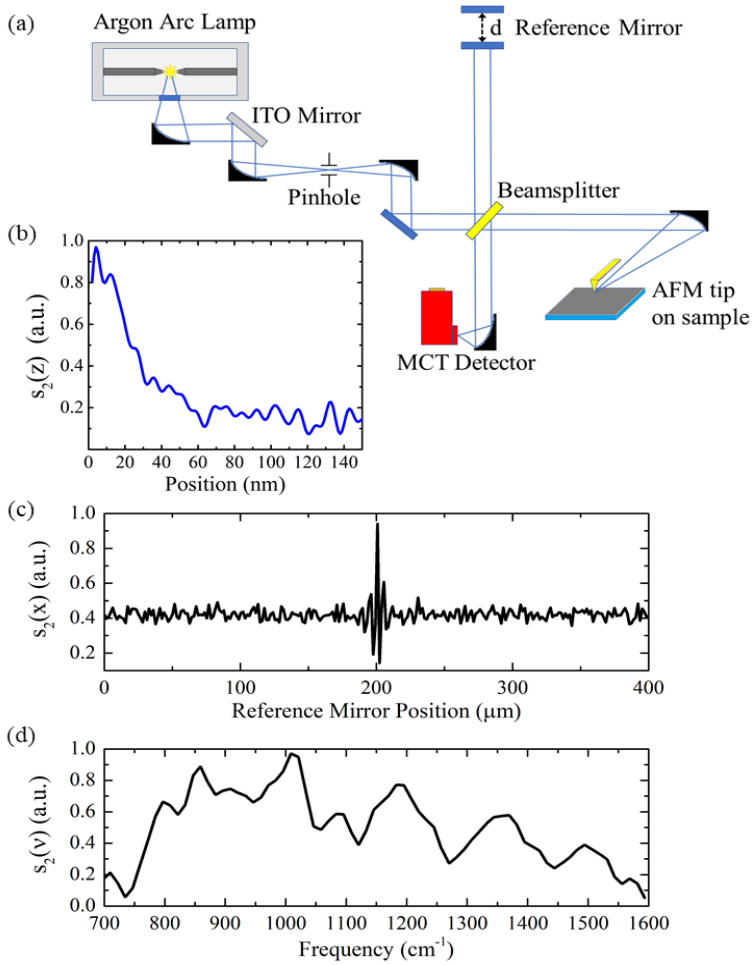

Fig. 3. (a) Schematic of the beam path used. (b) Approach curve obtained at the second harmonic with the reference arm set to the white light position (position of the peak in (c)). (c) Near-field interferogram on gold demodulated at the second harmonic obtained with the argon plasma light source and optical setup shown above and (d) the resultant spectrum generated by fast Fourier transformation of the interferogram.

The AFM is operated in tapping mode which modulates the infrared signal at the tapping frequency and higher harmonics of our tip. The tapping frequency (Ω) of the Arrow-NCPt is ~240 kHz while the tapping frequency of the PPP-NCSTAu is ~120kHz. Since the near-field signal scales non-linearly with tip-sample distance, it is also present in the higher harmonics (nΩ) of the cantilever oscillation frequency. The far-field background scattering from the tip-cantilever-sample system is suppressed by demodulating our signal at higher harmonics of the cantilever oscillation frequency [3]. We demonstrate that we exclusively measure the near-field signal by taking an approach curve on gold which is shown in Fig. 3(b). This approach curve is obtained by setting the reference arm to the white light position (the position of maximum constructive interference), and recording the signal as we retract the sample away from the tip. This demonstrates the expected non-linear decay in the near-field infrared signal (s_2) demodulated at the second harmonic of the AFM tip oscillation frequency. To record our spectra on gold, Si, SiO_2 and STO, we move the reference mirror a total distance of 400 μm i.e. 200 μm on both sides of the white light position. This leads to an optical path difference of 400 μm yielding a spectrum with a resolution of 25 cm^{-1}. Figure 3(c) shows an

Optics EXPRESS

interferogram recorded over gold with the Arrow-NCPt tip and Kolmar photovoltaic MCT. Fourteen scans were averaged with a 200 ms reference mirror step time taking 256 total data points per scan resulting in a total acquisition time of ~12 minutes. Figure 3(d) is the resultant spectrum generated by fast Fourier transformation of the interferogram.

3. Results

Firstly, we demonstrate that the spatial resolution of our setup is on the order of the AFM tip diameter and not limited by the diffraction limit of the tip illumination wavelength. We set the reference arm to the "white light position" i.e. the position of maximum constructive interference. We then take an AFM topography scan (Fig. 4(a)) across the edge of 100 nm of SiO_2 on silicon. The second harmonic of our near-field signal is simultaneously recorded (Fig. 4(b)). Although SiO_2 has a phonon-polariton resonance, the total integrated signal of silicon is higher than the total integrated signal of SiO_2. This contrast can be explained by the higher average refractive index of silicon (in the wavelength range of the incident infrared radiation) when compared to SiO_2 [13]. By taking a line trace across this border we see that while the topography line trace (Fig. 4(c)) shows a decrease in height when going from SiO_2 to Si, the near-field signal (Fig. 4(d)) has a sharp increase within about 50 nm, well below the diffraction limit of the range of mid-infrared wavelengths that are illuminating the tip.

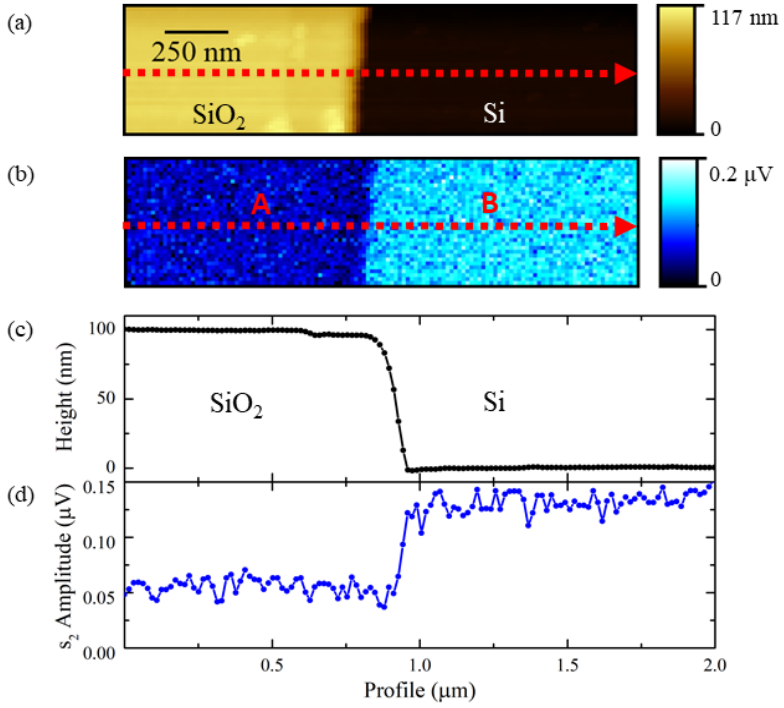

Fig. 4. (a) Topography and (b) the second harmonic near-field amplitude at the white light position obtained simultaneously on 100 nm thick SiO_2 on silicon. Each pixel represents an area of 15 square nanometers. The total integrated signal over all wavelengths is higher for silicon so it will have a higher amplitude in the near-field scan. (c) represents a line trace (red dashed line) averaged over 4 consecutive horizontal lines on the topography scan while (d) represents the same location for the near-field scan. In (d) we can see that moving off the SiO_2 step and onto the Si substrate there is a sharp increase in signal over about 50 nm which is about two orders of magnitude below the diffraction limit of the tip illumination wavelength range. The change in the near-field signal is solely due to the difference in the dielectric function of Si and SiO_2 and not due to a change in the height between the two materials.

Optics EXPRESS

To demonstrate the APLS capability as a broadband light source for nano-spectroscopy, the tip was centered at the positions indicated by the red letters in Fig. 4(b). Figure 5 represents the spectrum of SiO_2 normalized to a Si reference spectrum. Data was obtained at the second harmonic demodulation using a 15 nm radius tip with a tapping amplitude of 65 nm, and spectral resolution of 25 cm^{-1}. The near-field infrared amplitude (Fig. 5(a)) shows the well-known phonon polariton that peaks at 1130 cm^{-1} agreeing well with other measured results [7,13,15]. We are also able to resolve phase data (Fig. 5(b)) with our nano-spectroscopy setup and both our amplitude and phase data have the expected semi-quantitative agreement with the point dipole model and finite dipole model [3,28].

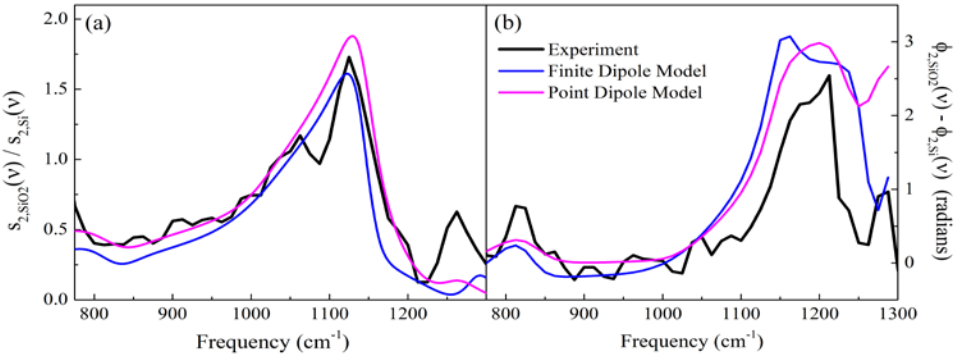

Fig. 5. Near-field amplitude (a) and phase shift ϕ (b) of 100 nm of SiO_2 normalized to Si. The location of these point spectra are represented approximately by the red letters in Fig. 3(b). The SiO_2 spectra were collected at point A and normalized to a spectrally flat silicon spectrum taken at point B. Comparing the experimental data (black) to the point dipole model (magenta) and finite dipole model (blue) we can see a semi-quantitative agreement.

To study the near-field spectrum of STO with reference to gold, 70 nm of gold was deposited on to a portion of a bulk STO substrate. The STO amplitude and phase shift were acquired and then normalized to data from the gold film. Here we used a 50 nm radius tip, 75 nm tapping amplitude, and spectral resolution of 25 cm^{-1}. The STO near-field amplitude and phase shift data is plotted in Fig. 6 with the inset in Fig. 6(a) demonstrating that we can see the resonance in the second, third, and fourth harmonics. Due to the significant suppression of the background at these higher harmonics, we can conclude that the peak is a near-field resonance. A peak in the normalized near-field infrared amplitude is seen around 640 cm^{-1} in Fig. 6(a). The finite dipole model matches the experimental amplitude better than the point dipole model. However, the experimental phase shift plotted in Fig. 6(b) is in better agreement with the point dipole model. The quantitative differences between the experiment and the models can be attributed to one or more of the following reasons: the more prominent noise level in this spectrum due to the lower signal-to-noise from the wider band photoconductive MCT; atmospheric absorption due to water vapor and CO_2 below 700 cm^{-1}; the 25 cm^{-1} spectral resolution; the models being simplified versions of tip-sample near-field interaction, and hence only giving a semi-quantitative estimate of the magnitude and position of the near-field resonances; and the uncertainty in the measurements of the dielectric function of STO in published sources. Note that our experimental data shows a clear resonance peak, and to our knowledge, this is the first experimental demonstration with S-SNOM of a near-field phonon polariton resonance in STO.

Optics EXPRESS

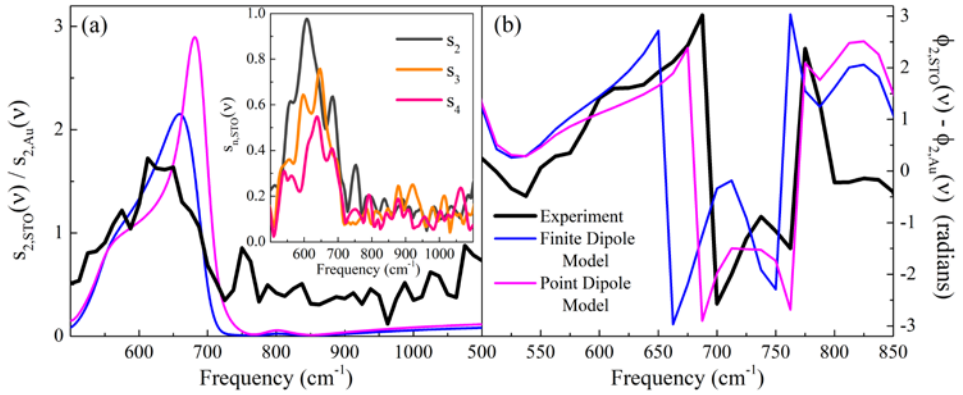

Fig. 6. (a) Phonon polariton resonance of STO normalized to a gold reference (black) compared to the point dipole model (magenta) and finite dipole model (blue). In the inset we show the non-normalized second, third, and fourth harmonic near-field spectra on STO demonstrating that this resonance persists in the *h*igher harmonics. (b) Phase shift of the near-field infrared signal on STO normalized to the gold reference and compared to the point dipole model (magenta) and finite dipole model (blue). The phase shift is constrained to values between π and -π.

4. Summary and outlook

With the introduction of our APLS, we have demonstrated that it is a highly broadband infrared light source capable of being used for nano-spectroscopy from the far-infrared to the mid-infrared spectral range. Sub-diffraction limit point spectra and near-field images were obtained at the second harmonic optical demodulation demonstrating the phonon-polariton resonance in SiO_2 with very good agreement consistent with previously published literature. The expected phonon-polariton that occurs in bulk STO was experimentally observed to occur around 640 cm^{-1}. We have demonstrated that our nano-spectroscopy set up can take spectra down to 500 cm^{-1}, the cutoff imposed by the ZnSe beamsplitter. Currently the upper limit seems to be the atmospheric absorption bands which occur above 1400 cm^{-1}. Future improvements that will be implemented include enclosing the entire near-field set up in dry, CO_2-free air. This will reduce atmospheric absorption and will extend our spectral range past the atmosphere lines above 1400 cm^{-1}. Moreover, there is potential for implementing other combinations of detectors, beam-splitters, and infrared transparent windows in the future to explore the spectrum of the APLS in the sub-500 cm^{-1} spectral range. This will enable acquisition of near-field spectra of lower frequency phonons in many materials.

Funding

National Science Foundation (NSF) (DMR-1255156).

Acknowledgments

The authors thank Dennis Manos for sharing his insights into plasma lamp technology and for his encouragement throughout this project. MMQ and TJH acknowledge stimulating discussions on infrared sources and detectors with David Tanner and G. Larry Carr. The authors also thank Tobias Gokus, Andy Huber, and Florian Huth of Neaspec GmbH for their technical support for the S-SNOM instrumentation. Thanks are due to William Henninger and John Bensel of the William & Mary machine shop who machined several parts for the argon plasma light source based on the designs prepared in the Qazilbash research group.